Available online at www.sciencedirect.com
ScienceDirect
Journal of Nuclear Materials 363–365 (2007) 1429–1435
journal of nuclear materials
www.elsevier.com/locate/jnucmat

Two-dimensional density profile measurement with a sheet thermal Li beam on CPD

H. Zushi [a,*], T. Morisaki [b], Y. Inada [c], J. Bouchard [d], K. Nakashima [c], H. Tsuchiya [b], K. Hanada [a], K. Sasaki [c], R. Bhattacharyay [c], K.N. Sato [a], K. Nakamura [a], M. Sakamoto [a], H. Idei [a], M. Hasegawa [a], S. Kawasaki [a], H. Nakashima [a], A. Higashijima [a]

[a] *RIAM, Kyushu University, Kasuga, Fukuoka 816-8580, Japan*
[b] *National Institute for Fusion Science, Toki 509 5292, Japan*
[c] *Interdisciplinary Graduate School of Engineering Science, Kyushu University, Kasuga, Fukuoka 816 8580, Japan*
[d] *Ecole Polytechnique, Japan*

Abstract

A sheet thermal Li beam to study the density contour near X-point and divertor strike points has been developed for the spherical tokamak CPD. The CCD camera with a time resolution of 1 ms and spatial resolution of ~1 mm can record two-dimensional images of LiI resonance line (300 mm × 500 mm). The performance of the sheet beam is absolutely calibrated by a quartz crystal monitor. The Li flux of 10^{18}–10^{19} m^{-2} s^{-1} is achieved near the X-point. The sheet characteristics of beam width and uniformity are also confirmed. This technique is applied during plasma initiation and electron cyclotron heating phase of plasma in a simple torus with a small vertical field. The formation of vertically stretched plasma at the position of the cyclotron resonance is clearly found. The expansion process towards the low field side is observed and an over dense plasma (>1×10^{18} m^{-3}) is obtained. A model calculation of LiI emission with density range of 1–5 × 10^{18} m^{-3} agrees fairly well with the observations. Over dense plasma formation is also discussed.

PACS: 52.50.Sw; 52.55.Fa; 34.50.Fa

Keywords: Lithium beam; Edge plasma; Divertor diagnostics

1. Introduction

In order to realize the most economical fusion reactor a conceptual design study based on a steady state spherical tokamak (ST) has been proposed [1]. The keys are a steady-state current drive and power as well as particle handling in this configuration. The possibilities of current ramp up and steady state ST operation have been demonstrated in the small ST device LATE [2], in which a ST plasma is produced solely by electron cyclotron heating (ECH) without center solenoid. Another problem is the

* Corresponding author. Fax: +81 92 573 6899.
E-mail address: zushi@triam.kyushu-u.ac.jp (H. Zushi).

0022-3115/$ - see front matter © 2007 Elsevier B.V. All rights reserved.
doi:10.1016/j.jnucmat.2007.01.259

plasma wall interaction (PWI) in ST configuration. So far a steady state tokamak operation has been performed in TRIAM-1 M using lower hybrid current drive (LHCD) in the limiter configuration. The strong local interaction between the lost energetic electrons and limiters has been considered one of the reasons for plasma termination [3]. Thus aiming at investigation for PWI in a steady state divertor ST configuration a small ST device, compact plasma wall interaction experimental device (CPD), has been built.

A two-dimensional density diagnostic system with a sheet Li thermal beam [4–7] has been installed to investigate the current start up physics, associated with the configuration change from an RF produced simple torus with a weak mirror field to a closed ST configuration, and the PWI near the X-point and divertor leg region. In this paper the process from plasma initiation to the over dense plasma formation is reported in a simple torus with a small negative decay index $n^* \equiv -\frac{R}{B_V}\frac{\partial B_V}{\partial R}$. The arrangement and the performance of the sheet Li beam will be presented in Section 2. The physics of RF break down and over dense plasma formation have been investigated in RF plasma with the sheet Li beam in presence of the toroidal magnetic field and a weak poloidal magnetic field and will be discussed in Section 3. Analysis for the over-dense plasma will be discussed in Section 4. Finally a summary will be given.

2. Arrangement and performance of the 2D image system

2.1. Arrangement of Li injector and CCD camera

CPD is a compact ST device whose major (R_0) and minor (a_0) radii are 0.3 m and 0.2 m, respectively. The bird's-eye view of CPD is shown in Fig. 1. Since there are four toroidal coils, and the return coils are located far from the plasma area, the ripple is tolerable (~8% at $R = 0.5$ m). The maximum current for each coil is 90 kA, which can produce $B_t = 0.25$ T at R_0. A set of 8.2 GHz klystrons (8×25 kW, CW) is used for ECH. Linearly polarized microwaves are injected through the rectangular horn antenna below the equatorial plane with an injection angle of ~15° from the normal direction to the toroidal field lines. In these experiments 2–80 kW power is used to initiate the RF plasma. An expansion process in presence of the weak poloidal field is investigated with this sheet beam.

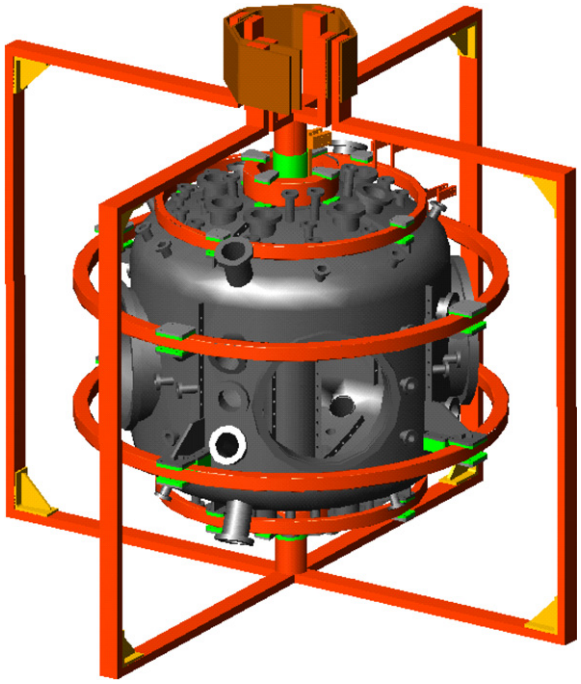

Fig. 1. Bird'-eye view of CPD. The coils are shown in red.

In order to investigate the density contour in the lower half of the CPD plasma a two-dimensional density imaging system (300 mm × 500 mm) is installed which is composed of a sheet Li beam injector and a CCD camera (Plxelfly qe) equipped with an optical filter (670.8 ± 5 nm). The Li beam injector is located at the bottom of the chamber and the beam is injected at an oblique angle of 18.18° at $R \sim 0.29$ m with respect to the machine axis, as shown in Fig. 2. The distance from oven to the X-point is ~0.5 m and the CCD camera has a tangential view into the chamber. The 2D image (boxed area) can be recorded for 1–2 ms typically with 1280×1024 pixels with a size of 6.7 μm × 6.7 μm. The CCD readout time is ~40.3 ms by pixel binning. A lens (PENTAX B1214D-2) whose focal length is 12.5 mm and F–number is 1.4 is attached in front of the CCD. The special resolution is ~1 mm. When an incident angle of the light deviates from the normal direction to filter surface, the transmission efficiency of the optical filter is reduced and the peak of the filtered wavelength is down shifted. The edge region of the boxed area is hence interfered by H_α emission. Assuming plasma reproducibility with and without Li injection the CCD image is obtained.

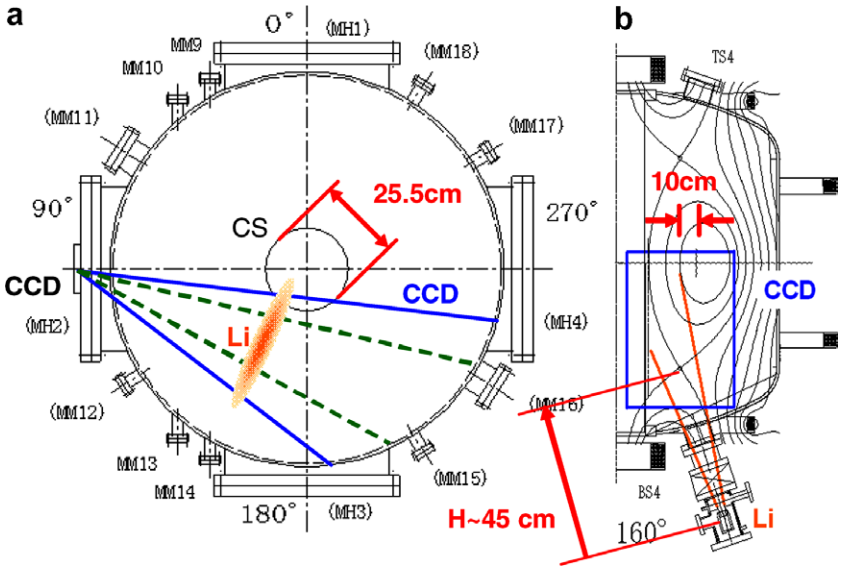

Fig. 2. Arrangement of Li injector and CCD detection system: (a) top view of CPD and (b) side view including the typical magnetic surfaces.

2.2. Performance of the sheet Li beam

The specification of the sheet thermal beam is calibrated with a quartz crystal deposition monitor (QCM; INFICON 008-010-G10) from the decrease in frequency of the quartz oscillator from 6 MHz to 4.5 MHz. Since the effective size of the quartz crystal is ~8 mm ϕ, the deposition flux (or evaporated Li flux (Γ_{Li})) is evaluated from the Li film thickness and operation duration (usually 3 min). The oven is heated with a sheath heater ranging from 450 °C to 630 °C and Γ_{Li} is extracted through an array of 11 collimated holes, each of diameter 3 mm and is shaped through a rectangular slit (35 mm × 6 mm), whose longer side is aligned with the major radius of CPD. The deposited Li thickness is measured with the QCM and thus Γ_{Li} is determined. Γ_{Li} at the center of the sheet beam is 10^{18}–10^{19} m^{-2} s^{-1} for the range of usual oven temperature (T_{oven}) from 525 °C to 630 °C at a distance of 470 mm from the slit. A T_{oven} dependence of Γ_{Li} is shown in Fig. 3(a). Since the mean velocity of Li atom at $T_{oven} = 527$ °C is ~700 m/s, the Li atom density is evaluated ~1.4×10^{15} m^{-3} near the X-point region. By scanning the crystal sensor by ±20 mm across the rectangular beam at the fixed position, the characteristics of the sheet beam are evaluated. The uniformity of ±10% of Γ_{Li} is achieved for 40 mm along the long side of the rectangular slit (along the major radius) and the full width at half maximum is found to be ~40 mm along the short side of the rectangular slit (along the toroidal direction), as shown in Fig. 3(b) and (c). By comparison with the Monte Carlo calculations the uniformity for 150 mm is expected in the major radius direction.

3. Experimental results

3.1. Experimental condition and plasma initiation

Linearly polarized microwaves are injected in the X-mode from the outboard side at oblique angles, being tilted by ~15° with respect to the major radius. In addition the O-mode is also injected. Power ratio is 0.6(X):0.4(O). The toroidal coil current is raised linearly from $t = 0$ s up to 50–60 kA in $t = 0.1$ s and is kept constant until $t = 0.3$ s. During the B_t ramp-up phase the vertical field B_v is also raised up to 15 Gauss at $R \sim 0.3$ m. An initial plasma is instantly produced at the R_f power of ~2 kW when the position of the fundamental EC resonance ($B_{res} = 0.293$ T at R_{res}) shifts just outside the center stack ($R \sim 0.11$ m). Although at this break down phase the plasma stretches vertically as it is found by a fast camera, the vertically stretched LiI light contour is limited by the vertical width of the beam. It is found that the break down occurs at $R_{res} = 0.12$ m at which the cover plate is attached to protect the center stack within

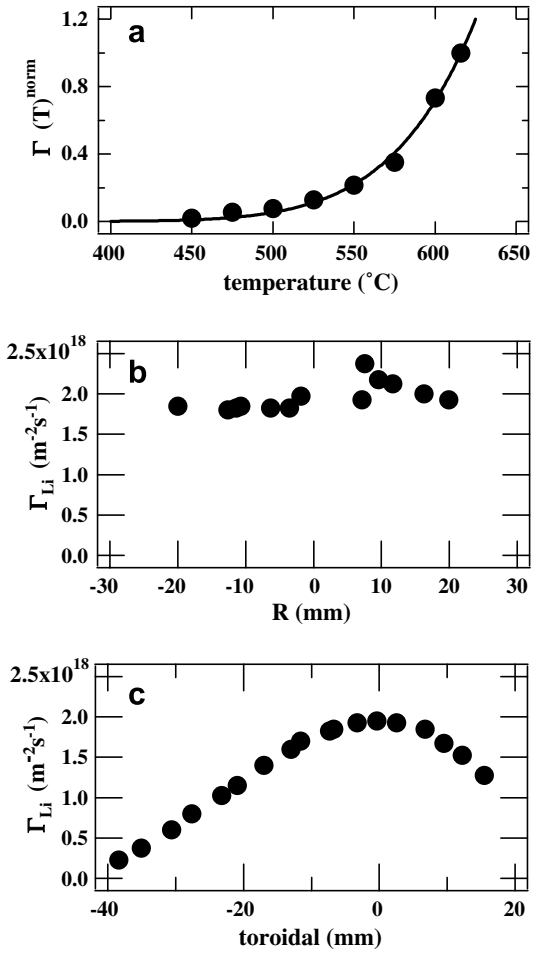

Fig. 3. The performance of the sheet Li beam: (a) dependence of T_{oven} on Γ_{Li} . Theoretical curve normalized at $T = 616$ °C is also plotted. (b) Uniformity of Γ_{Li} along the major radius, (c) beam width in the toroidal direction. The data are taken at 470 mm away from the shutter.

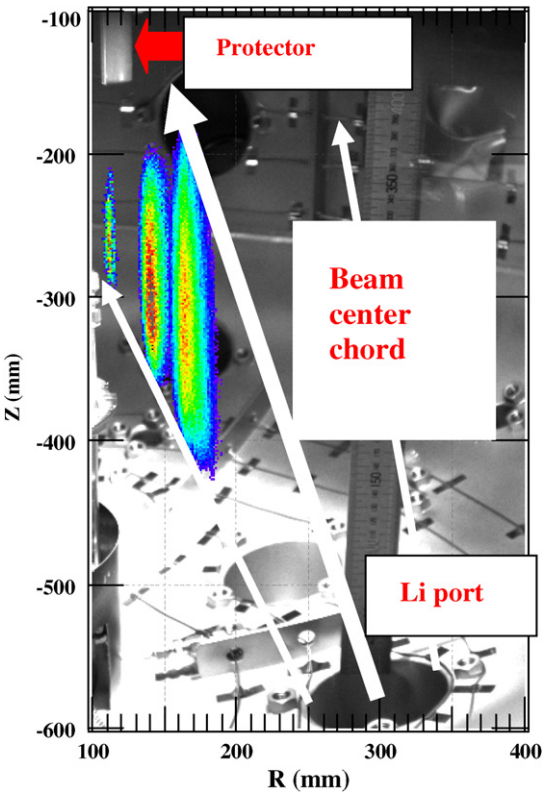

Fig. 4. 2D images of LiI during the plasma initiation phase. Three snap shots at different B_t fields are superposed to the picture of the chamber. The exposure time is 2 ms. Three arrows indicate the central chord of the Li beam and both left and right boundaries.

±150 mm from the mid plane, as shown in Fig. 4. It is confirmed that the radial peak position of this initial LiI contour corresponds well to the position of the fundamental cyclotron resonance.

3.2. Rapid plasma expansion at high RF power

It is observed that plasma quickly expands towards the low field side when RF power is increased at $t \sim 0.15$ s from 2 kW (4th image) to 50 kW (5th–7th) at the constant B_t and B_v fields. The H_α and OII intensities viewed along the major radius on the mid plane remain almost constant during the plasma expansion phase. Fig. 5 shows three successive (4th–6th) images taken every ~ 45 ms. The core of 4th image corresponds to the resonance position $R = 0.164$ m ($B = B_{res}$) and therefore the contour is vertically elongated. The bottom side of the contour is limited by the lower edge of the Li beam and the upper side by the reduction of the transmission efficiency of the filter. The 5th image shows that the contour is asymmetric with respect to the beam central chord, which means that the plasma with higher density is expanding from the resonance position to the right, but for $R > 0.3$ m the density is lower. The position of the second harmonic cyclotron resonance is located at $R \sim 0.32$ m. At $t \sim 0.2$ s B_v is raised rapidly up to 45 Gauss and it is decayed to 15 G at 0.25 s. The decay index is ~ -0.06 at $R \sim 0.25$ m. A relatively symmetric contour (6th image) is achieved, however, a high density area whose radius is a few cm is observed just above the Li injection port. The 7th image at $t \sim 0.27$ s shows an asymmetry contour similar to the 5th one, because B_v is decreased to ~15 G.

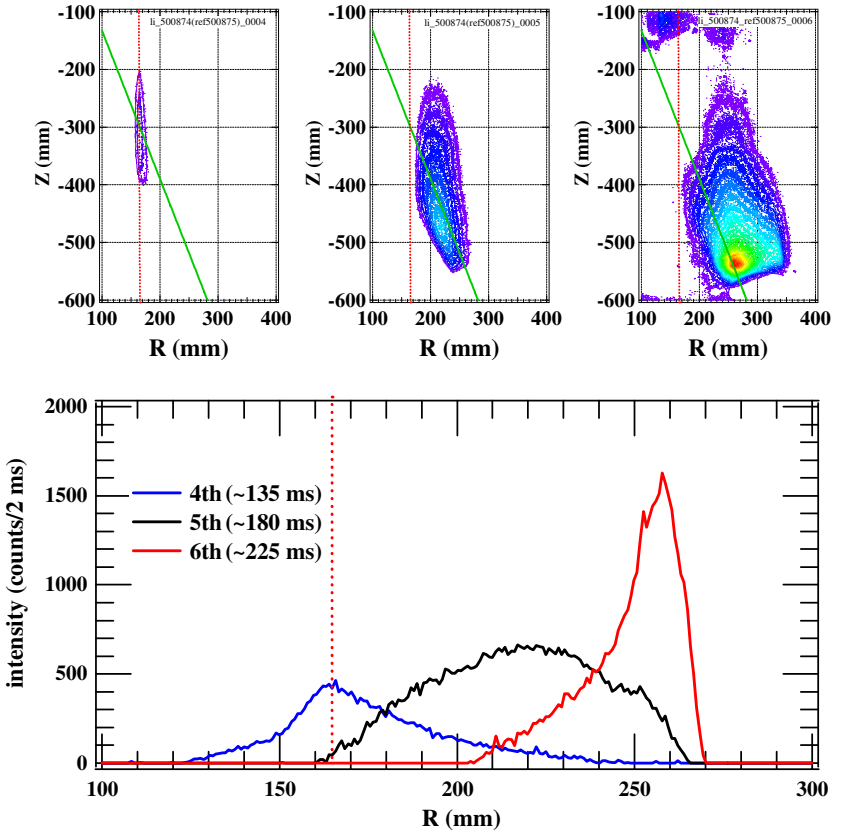

Fig. 5. (Top) 2D images of LiI in the phases of the plasma initiation and the plasma expansion. The intensity contour level is fixed. On 6th image a bright area near the left top is due to H_α. The vertical dotted line corresponds to the cyclotron resonance layer. (bottom) The LiI line intensities along the green line (top) are plotted as a function of the major radius. The unit of the vertical axis is counts per 2 ms.

The LiI intensity profiles from 4th to 6th along the green line are shown as a function of R. The peak of the LiI profile moves towards to the lower field side. The vertical dotted red line corresponds to the fundamental cyclotron resonance position.

3.3. Reconstruction of the density profile

According to Ref. [7] the density is reconstructed evaluating to the following equation:

$$n_e(s) = \frac{v_b}{\langle \sigma v \rangle_{ion}} \frac{I_{Li}(s)}{\int_s^\infty I_{Li}(s)ds},$$

where s indicates the beam path. $I_{Li}(\infty) = 0$ is assumed and the *velocity* distribution of the thermal beam is neglected. The thermal velocity at $T_{oven} = 527$ °C is used as v_b. The electron temperature is assumed to be 10 eV and the rate coefficient $\langle \sigma v \rangle_{ion}$ by electron impact ionization is 6.5×10^{-14} m^3/s. The results are shown as a function of R in Fig. 6. In the initial phase the density is $\sim 0.25 \times 10^{18}$ m^{-3} at R_{res} and a decay length of the density profile is about 1.5 cm near R_{res}. After the RF power is increased, the density at $t \sim 0.18$ s is above 0.6×10^{18} m^{-3}at R_{res} and two folded profile is observed. The decay length near R_{res} becomes

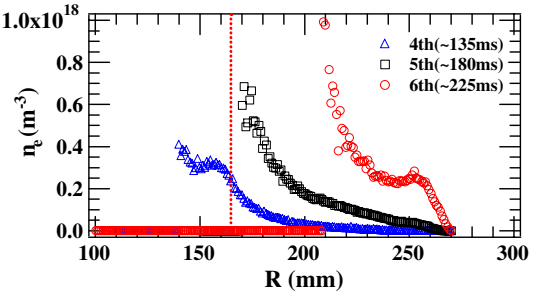

Fig. 6. Reconstructed density profiles at different times but along the same beam path as indicated by the green line in Fig. 5. Around $R \sim 0.27$ m the density gradient becomes steep in time, suggesting high-density plasma expansion.

2–3 cm. The density at $t \sim 0.225$ s is further increased when B_V is 30 G. The high dense plasma with $n_e \sim 0.2 \times 10^{18}$ m^{-3} is achieved just above the Li injection port and n_e reaches to 1×10^{18} m^{-3} at $R \sim 0.2$ m. In addition to the plasma expansion since there is no the LiI emission near R_{res}, it should be noted that the global plasma density increases for $R < 0.2$ m.

4. Discussion

4.1. Model calculation of the LiI profile with an assumed density profile

Since the reconstruction procedure causes the numerical difficulty to decide the density where $I_{Li}(s)$, $\int_s^\infty I_{Li}(s)ds$ are small, and the uncertainty in T_e causes the ambiguity in n_e through $\langle\sigma v\rangle_{ion}$, the following technique is used to deduce the density near the resonance region. Since absolute calibration has been done for the CCD camera by using a standard Xe lamp (L7810 Hamamatsu), the counts of the CCD within 2 ms are modeled and line profiles are compared with Fig. 5. Absolute value and the profile width are sensitive to the ionization mean free path and attenuation of the Li atoms and the rate coefficient for the excitation is also a function of T_e when T_e is below 10 eV [7]. A model profile for n_e, attenuation of the Li density n_{Li} and counts per 2 ms C_{Li} converted from the light intensity are as follows:

$$n_e(R) = n_e(R_p)\exp\left(-\frac{|R-R_p|}{\lambda}\right)$$
$$(R > R_p\ \lambda = \lambda_{out},\ R < R_p\ \lambda = \lambda_{in}),$$
$$n_{Li}(R) = n_{Li}(R_a)\exp\left(-\int_{Ra}^{R} n_e(R)\langle\sigma\rangle_{ion}/v_b dR\right),$$
$$C_{Li}(R) = K_{calib} n_e(R) n_{Li}(R)\langle\sigma v\rangle_{exc} h\nu \frac{\Delta\Omega}{4\pi} V_p,$$

where R_p is the peak density position, $\lambda_{out,in}$ the characteristic lengths for the density profile, $\langle\sigma v\rangle_{ion}$ ($=6.5 \times 10^{-14}$ m^3/s at $T_e = 10$ eV) the ionization rate coefficient, v_b the beam velocity evaluated at $T_{oven} = 527$ °C, $\langle\sigma v\rangle_{exc}$ the excitation rate coefficient ($\sim 9 \times 10^{-13}$ m^3/s at $T_e = 10$ eV), $\Delta\Omega$, the solid angle, V_p plasma volume, and K_{calib} is the calibration factor at $\lambda = 670.8 \pm 5$ nm. $n_{Li}(R_a)$ is calculated from the measured Γ_{Li} and v_b. All these magnitudes are assumed to be constant. For model density profiles in Fig. 7(a) $n_e(R_p) = 1$–3×10^{18} m^{-3} and $\lambda_{out} = 2$ cm, and $n_e(R_p) = 5 \times 10^{18}$ m^{-3} and $\lambda_{out} = 5$ cm are used. In Fig. 7(b) the results of C_{Li} (R) are shown and their profiles and absolute values agree fairly well with those in Fig. 5. According to these model calculations the peak density is expected to be 1–5×10^{18} m^{-3}.

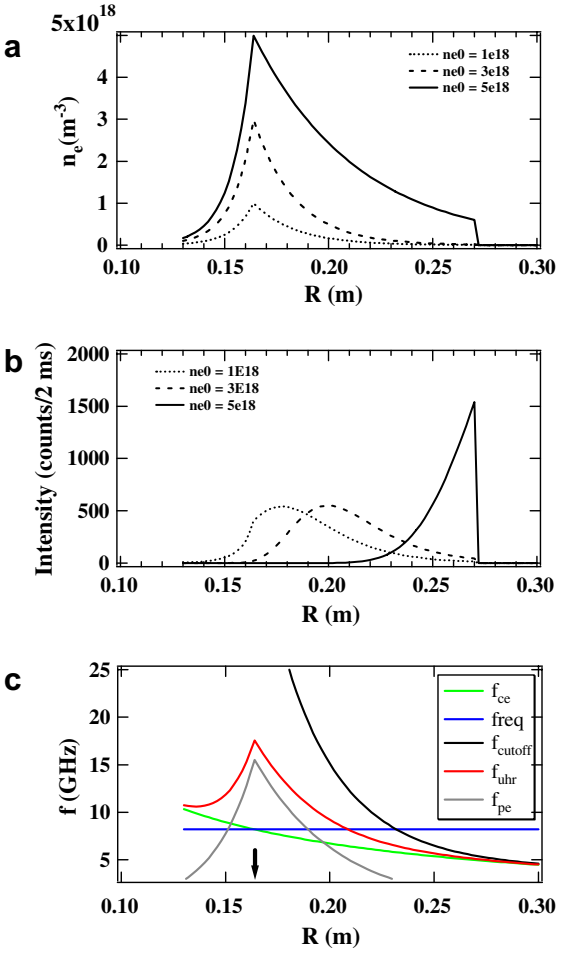

Fig. 7. (a) The model exponential density profiles with decay length λ_{out} of 2–5 cm and n_{e0} of 1–5×10^{18} m^{-3} and (b) calculated LiI emission profiles. The width of the LiI and the absolute values agree fairy well with those in Fig. 5. (c) Characteristic frequencies (f_{ce}, f_{UH}, f_{cutoff},f_{pe}) as a function of R for a model density profile with 3×10^{18} m^{-3}. The blue line is 8.2 GHz and intersecting points indicate the cutoff or mode conversion and resonance positions. The cutoff layer expands to the low field side, which shields the propagation of the X-mode and the plasma cutoff prevents the O-mode waves approaching to the cyclotron resonance layer.

4.2. Wave characteristics and over-dense plasma

2D images give us a new insight of the plasma initiation and expansion process. Although these

processes have been considered to be important for current ramp up [2], *a* similar behavior is found even in a simple torus with small B_v without plasma current. Fig. 7(c) shows four layers of right hand cutoff (black), upper hybrid resonance (red[1]) , fundamental (green) and plasma frequency (grey) as a function of R. The same density profile with $n_e(R_p) = 3 \times 10^{18}\ m^{-3}$ as considered in Section 4.1 is used. The cutoff position is calculated with an assumption of R dependence of the parallel refractive index $N_{\|}$. Since the cyclotron resonance is shielded by the cutoff layer expanding towards the lower field side and the cutoff layer exists vertically just above the chamber wall, no absorption and no bypass of X-mode are simply expected. Since the electric field vector in the linear polarized waves is slightly tilted, the contribution of the O-mode component should be considered. However, since the cutoff density of the O-mode is $\sim 7 \times 10^{17}\ m^{-3}$, the obtained plasma with the density $>1 \times 10^{18}\ m^{-3}$ is also the over-dense plasma for the O-mode. The mode conversion from the X-mode to electron Bernstein wave or from the O-mode to electron Bernstein wave via X-mode conversion is one of candidates to heat and sustain the over-dense plasma.

5. Summary

A sheet thermal Li beam system equipped with a CCD camera attached to an optical filter for LiI line has been installed to measure two dimensional density profiles in the spherical tokamak CPD. 2D images (300 mm × 500 mm) are recorded with a temporal and a spatial resolution of 1 ms and ~1 mm, respectively. The value of Γ_{Li} is absolutely measured via the thickness of the Li film deposited on a quartz crystal exposed to the beam. Li flux density of $\Gamma_{Li} = 10^{18}$–$10^{19}\ m^{-2}\ s^{-1}$are achieved at a distance of 0.5 m from the collimator. The beam width is 40 mm in the toroidal direction, and uniformity is confirmed to be better than 15% over the radial direction for 40 mm. The plasma initiation and evolution are investigated in ECRH plasma in a simple torus with a small B_v. The formation of a vertically stretched plasma with a width of few cm is observed at R_{res}. During the expansion process towards the low field side higher plasma density ($>1 \times 10^{18}\ m^{-3}$) is achieved. With increased B_v the density is found to increase $\sim 5 \times 10^{18}\ m^{-3}$. The X–B/O–X–B mode conversion for over dense plasma production is discussed.

Acknowledgements

This work has been partially performed under the framework of the bi-directional collaboration organized by NIFS. This work is partially supported by a Grant-in-Aid for Scientific Research from Ministry of Education, Science and Culture of Japan.

References

[1] H.R. Wilson et al., Nucl. Fusion 44 (2004) 917.
[2] T. Maekawa et al., Nucl. Fusion 45 (2005) 1439.
[3] H. Zushi et al., Nucl. Fusion 45 (2005) S142.
[4] P. Bogan et al., J. Nucl. Mater. 128&129 (1984) 157.
[5] U. Samm et al., J. Nucl. Mater. 162–164 (1989) 24.
[6] K. Komori et al., J. Appl. Phys. 30 (1991) 3526.
[7] A. Huber, U. Samm, B. Schweer, Ph. Mertens, Plasma Phys. Control. Fus. 47 (2005) 409.

[1] For interpretation of the references to colour in Figs. 1, 2, 4–7 the reader is referred to the web version of this article.